RSC Advances

ROYAL SOCIETY OF CHEMISTRY

www.rsc.org/advances

Biomimetic mineralization of anionic gelatin hydrogels: effect of degree of methacrylation†

Lei Zhou[a], *Guoxin Tan*[a],*, *Ying Tan*[a], *Hang Wang*[a], *Jingwen Liao*[b], *Chengyun Ning*[b],*

[a] School of Chemical Engineering and Light Industry, Guangdong University of Technology, Guangzhou, 510006, China

[b] College of Materials Science and Technology, South China University of Technology, Guangzhou, 510641, China

†Electronic supplementary information (ESI) available. See DOI: 10.1039/b000000x/

Corresponding Author

*Guoxin Tan; *Chengyun Ning

E-mail: tanguoxin@126.com (G.T.); imcyning@scut.edu.cn (C.N.)

ABSTRACT

The mineral-polymer composite materials have been used as artificial bone grafts and scaffolds in bone tissue engineering. Polymer-controlled mineralization is effective to fabricate such composites. In this study, we synthesized organic-inorganic composites using anionic gelatin methacrylate (GelMA) hydrogels containing a high percentage of Ca^{2+} binding-carboxyl groups as a template for mineralization. Homogeneous surface and interior carbonated hydroxyapatite were achieved on the resulting mineralized porous hydrogel composites, and were confirmed to resemble apatite-like structures. The effect of crosslinker content on mineralization was examined using GelMA hydrogels with different degrees of methylacrylation (DM). It was found that increasing the DM of the hydrogel suppressed the growth of carbonated hydroxyapatite layers, as was evident from the extent of calcification and morphology of the minerals. The dependency of the mineralization on hydrogel variables was related to the change in physicochemical properties of gel, including charge density, swelling. Compressive mechanical testing demonstrated that the compressive modulus and strength of the hydrogels increased with increasing DM and mineralization extent. Overall, mineralization of GelMA hydrogels with controllable mineral content and good mechanical properties provide a biomimetic route toward the development of bone substitutes for the next generation of biomaterials. The results of this study also provide insight into better understanding the role of hydrogel matrix on biomineralization.

Keywords: Biomimetic mineralization; Hydroxyapatite; Gelatin; Cross-linking; Hydrogel; Composite scaffold

1. INTRODUCTION

Bone material is an inorganic–organic nanocomposite. The inorganic hydroxyapatite nanocrystals are deposited on organic collagen fibrils, which possesses unique biological functions (*e.g.*, mineralization) and mechanical performance (*e.g.*, high strength and fracture toughness).[1, 2] Therefore, from a biomimetic point of view the development of synthetic bone substitutes mimicking mechanical and biological properties of natural bone is of great importance for enabling a range of applications in bone tissue engineering.[3-7]

In the context of biomimetic bone scaffolds, hydrogels are particularly promising material candidates. Hydrogels are 3D networks of hydrophilic polymer chains that have been widely used as scaffold materials in tissue engineering and regenerative medicine.[8] Their popularity is attributed to the beneficial properties such as high water content and biodegradability. In addition, it is desirable to easily modulate the physical, chemical and biological properties of hydrogels by varying a number of parameters such as the degree of the cross-links and the concentration, chemistry, and molecular weight of the precursors.[9-11] Nevertheless, it is observed in previous studies highly crosslinked hydrogel environments have greater mechanical stiffnesses but posed limitations in maintaining cell viability.[12, 13] Moreover, most of the synthetic hydrogels lack of osteoconductivity (*i.e.*, bone-bonding ability).[14]

To overcome above-mentioned shortcomings of a hydrogel alone approach toward bone regeneration, the development of bone substitutes based on hydrogel-mineral composites has been proposed. In that way, the beneficial properties of the hydrogel can be combined with the excellent osteoconductive and mechanical properties of calcium

phosphate (CaP) crystals. Several routes have been proposed for incorporation of inorganic materials into a hydrogel matrix including direct blending and grinding,[15] co-precipitation[16] and polymer-controlled mineralization.[17] Among them, polymer-controlled mineralization by a biocompatible aqueous solution is regarded as the more effective way. The morphologies and structures of hydroxyapatite produced from mineralization process are similar to the natural bone mineral, having important characteristics, such as low crystallinity, nanoscale sizes and being resorbable.[18]

To create a mineralized hydrogel composite with enhanced mechanical properties and improved biological affinity to living bone, we utilized photo-crosslinkable gelatin methacrylate (GelMA) acting as a template for hydroxyapatite deposition. Gelatin methacrylate (GelMA) is formed by adding methacrylate groups onto the amine-containing side groups of gelatin, which becomes a gelatin-based, photo-crosslinkable hydrogel.[19] Particularly, GelMA hydrogel contains gelatin as its backbone, which is an inexpensive denatured collagen derived from main part of the extracellular bone matrix. It is suggested that gelatin can offer nucleation sites that are quite similar to those of the biological matrix, which can induce the precipitation of hydroxyapatite.[17] Additionally, it has also been reported that anionic gelatin created by alkaline treatment has a high percentage of carboxylic groups.[9] Thus the anionic gelatin selected has a negatively charged surface, which are favorable for the heterogeneous nucleation of calcium phosphate.[20] Consequently, the GelMA hydrogel, due to the presence of anionic gelatin is expected as templates for growth of calcium phosphate.

There have been previous studies on the role of gelatin in the formation of apatite.[16, 21] But few studies investigated the potential effect of crosslinker of gelatin-based hydrogels

on the mineralization process, so it is still largely unknown how crosslinker in gelatin dictates the nucleation and mineral growth. There is a general consensus that physicochemical properties of hydrogels strongly affect the mineralization process. For example, Chaenyung et al[22] have demonstrated several matrix physicochemical properties including charge density, hydrophobicity, and pore size play vital roles in modulating composition and morphology of minerals formed within a 3D matrix. A typical approach for controlling hydrogel physicochemical properties is to mediate the network structure by altering crosslinker contents. We hypothesize that the crosslinker contents of the hydrogel can influence interactions between mineral and hydrogel interface, thereby regulate the hydroxyapatite mineralization outcome.

Therefore, this study examined the potency of photo-crosslinked polymethacrylate hydrogels containing anionic gelatin in templating 3D hydroxyapatite-mineralization. Furthermore, the effects of the degree of methacrylation (DM) on the mineralization process of GelMA hydrogel in 3D and, in turn, the influence of the mineralization on the mechanical properties of the biomimetic scaffolds were investigated. Thus, a series of photopolymerizable GelMA macromers with various DM were prepared and characterized, and proton nuclear magnetic resonance (^{1}H NMR) was used to confirm the DM. The nucleation, growth, and distribution of calcium phosphate on the surface and within the hydrogel were systematically investigated by varying DM of the hydrogel. Moreover, mechanical compression analysis was performed to investigate the changes of the mechanical properties due to the mineralization of the hydrogel scaffolds.

2. EXPERIMENTAL SECTION

2.1. Materials

Gelatin (Type B, 250 bloom from porcine skin), methacrylic anhydride (MA), 3-(trimethoxysilyl) propyl methacrylate (TMSPMA), phosphate buffered saline (PBS) and D_2O were obtained from Aladdin Industrial Co. Ltd. (Shanghai, China). The inorganic salts for mSBF were of analytical grade and purchased from Guangzhou Chemical Reagent Co. Ltd. (Guangzhou, China). The photoinitiator, 2-hydroxy- 1-[4-(hydroxyethoxy)-phenyl]-2-methyl-l-propanone (Irgacure 2959) and poly(dimethylsiloxane) (PDMS) were purchased from Sigma–Aldrich (USA). The UV curing system (Omnicure S1500) from EXPO Photonic Solutions Inc. (Ontario, Canada) was used for polymerization of hydrogels.

2.2. Synthesis of Methacrylated Gelatin

Details of the synthesis process of methacrylated gelatin have been reported previously.[23] Type B gelatin was dissolved at 10% (w/v) into PBS at 60 ℃. MA was then added to the gelatin solution at a rate of 0.5 mL min^{-1} while stirring at 50 ℃ for 3 h. The fraction of lysine groups reacted was modified by varying mass/volume ratios of MA/gelatin of 0.08, 0.40 and 1.00 (m/v) present in the final reaction mixture, in order to synthesize GelMA with low (Low-GelMA), medium (Medium-GelMA) and high (High-GelMA) degrees of methacrylation, respectively. After a 5-time dilution with additional warm PBS, the GelMA solution was dialyzed against ultrapure water using a 12-14 kDa cutoff dialysis tubes (Spectrum Laboratories) for 6 days at 50 ℃ to remove unreacted MA and additional by-products. The GelMA solution was frozen at -80 ℃, lyophilized and stored at room temperature until further use.

2.3. ^{1}H NMR

The chemical modification to gelatin was assessed by proton nuclear magnetic resonance (^{1}H NMR) spectroscopy. The gelatin and methacrylated gelatin were dissolved in D_2O at a concentration of 10 mg/mL and at a temperature of 50 ℃. ^{1}H NMR spectra were recorded with a Bruker Avance 400 spectrometer with a single axis gradient inverse probe. Three spectra were collected from each sample. The degree of methacrylation (DM) was defined as the ratio of methacrylate groups divided by of the free amine groups in gelatin prior to the methacrylation reaction, as previously described.[24]

2.4. Zeta Potential Measurement

The electrical surface charge property of synthetic GelMA samples was investigated by zeta potential measurements using a zeta potential analyzer (ZetaPALS, Brookhaven Instruments Corp, USA). Default settings on the ZetaPALS were used, *i.e.* dielectric constant, refractive index and viscosity were assumed to be the same as for water. The zeta potential was measured in water at 25 ℃ and pH 7 with an applied electric field strength of 26 V cm^{-1} for three measurements.

2.5. Hydrogel Preparation

Before use, a GelMA prepolymer solution was prepared by mixing the lyophilized GelMA macromer (10 w/v % final) and the photoinitiator (Irgacure 2959) (0.5 w/v %) in PBS at 80 ℃ until fully dissolved. To fabricate GelMA hydrogel disk (6mm in diameter, 700 μm in thickness), 53 μL of a prepolymer solution was pipetted into the cylindrical PDMS mold covered on a TMSPMA treated glass slide and then exposed to UV light (7.1 mW/cm^2, 360-480 nm) for 35 s at room temperature. After being detached from the

mold and glass slide, the resulting GelMA hydrogels were incubated for 12 h at 37 ℃ in PBS to remove excess uncrosslinked gelatin.

2.6. Swelling measurements

To assess gels swelling, the GelMA hydrogels were incubated in PBS at 37 ℃ for 24 h to reach equilibrium. Discs were removed from PBS and blotted with a KimWipe to remove the residual liquid and the swollen weight was recorded. Samples were then lyophilized and weighed once more to determine the dry weight of polymer. The mass swelling ratio was then calculated as the ratio of wet mass to the mass of dry polymer. Four samples were tested for each hydrogel.

2.7. Mineralization of the hydrogel

The various lyophilized hydrogel disks were first incubated in the modified simulating body fluid (mSBF) under vacuum conditions for 30 min to remove any air bubbles potentially trapped in the pores of the specimens. After degassing the samples, the mineralization reaction was kept in a 37 °C oven for 6 and 12 days. The mineralization solution was refreshed on a daily basis to supply a sufficient amount of ions. The mSBF contained 141 mM NaCl, 4.0 mM KCl, 0.5 mM $MgSO_4$, 1.0 mM $MgCl_2$, 4.2 mM $NaHCO_3$, 3.75 mM $CaCl_2$, and 1.5 mM KH_2PO_4. The pH of mSBF was maintained at pH 7.4 by adding Tris-HCl buffer.[25] After mineralization, the disks were thoroughly washed with ultrapure water to remove mSBF inside the hydrogels, lyophilized, and stored at room temperature until use.

2.8. Scanning Electron Microscopy (SEM) Analysis

Surface- and cross-sections of the lyophilized non-mineralized and mineralized GelMA hydrogel disks were prepared by the freeze–fracture technique and mounted on

aluminum stubs using a double-sided copper tape, then sputter coated twice with Pt/Pd. The morphology of samples was analyzed using a field-emission scanning electron microscopy (Nova Nano SEM 430, FEI) equipped with an energy dispersive X-ray spectroscopy (EDX) module (LinkISIS, Oxford) at 15 kV. For elemental analysis of mineralized samples, energy-dispersive X-ray spectroscopy (EDS) analysis was performed during SEM examination. To determine calcium and phosphate distribution within the bulk of the mineralized samples, line scans were analyzed on the cross-sections with a 15 kV accelerating voltage.

2.9. Transmission Electron Microscopy (TEM) Analysis

TEM was used to characterize the morphology and identify the crystalline form of the minerals inside the mineralized hydrogel sample. Mineralized samples were prepared for TEM analysis following the protocols performed on bone and naturally mineralized tendon by Weiner and Traub.[26] Briefly, the mineralized GelMA hydrogel were pulverized into a fine-grained powder in liquid nitrogen mortar and pestle, then dispersed in ethanol and added dropwise onto a 3 mm diameter carbon coated copper TEM grid. The samples were examined by JEOL JEM-2100HR TEM at 200 kV. Selected Area Electron Diffraction (SAED) was recorded using the same equipment.

2.10. X-ray Diffraction (XRD) Analysis

X-ray diffraction (D8 Advance, Bruker, Germany) of the specimens was performed using Cu Ka X-ray radiation (40 KV, 40 mA), in the 2θ range of 10-60°, with a step rate of 2°/min, and a sampling interval of 0.02°. The phase composition was assigned by comparing the acquired spectra with peaks identified in the International Center for Diffraction Data database.

2.11. Fourier Transform Infrared (FTIR) Analysis

For FTIR characterization, the unmineralized and mineralized GelMA hydrogels were grounded into powder in liquid nitrogen mortar and pestle, mixed with KBr (sample/KBr 1 : 100 w/w), and pressed into pellets. FTIR spectra were then recorded with an Avatar 380 FTIR spectrometer (Thermo Nicolet, USA) at room temperature from 400 to 4 000 cm^{-1} with a resolution of 4 cm^{-1}, using 32 scans.

2.12. Thermogravimetric Analysis and Differential Scanning Calorimetry (TGA/DSC)

To determine the degree of mineralization of the samples, TGA/DSC tests were conducted using a simultaneous thermal analysis (STA449C/3/MFC/G, Netzsch, Germany). A heating rate of 10 ℃ min^{-1} was applied in the temperature range of 30-800 °C under air environment. For TGA/DSC tests, lyophilized unmineralized and mineralized hydrogel samples were pulverized with a mortar and pestle while frozen in liquid nitrogen and about 10 mg of samples were used for examination. The mineral content was determined by the remaining at 600 °C after the organic portion of the samples was totally combusted.

2.13. Mechanical Testing

The effect of mineralization on scaffold mechanical properties was evaluated through unconfined compressive testing of GelMA hydrogels with various DM at days 6 and 12 conditioning in mSBF and compared to as made unmineralized hydrogels. All samples were preconditioned in PBS at room temperature for 12 h prior to testing. The compression tests were performed with a hydrated mineralized hydrogel disk sample, 6 mm in diameter, and 800 μm in thickness, which were subjected to testing at a rate of

20% strain/min on a Bose ELF 3200 universal testing system (Bose Corp., Eden Prairie, MN, USA) for compression testing. The compressive modulus was calculated from the stress-strain curves in the linear region corresponding to 5-15% strain. Three samples were tested for each hydrogel. The results are presented as mean ± standard deviation.

One way ANOVA tests using one way Anova tool were performed on mechanical testing using software SPSS v19.0.0 (IBM, NY) to determine whether a significant difference exists ($p < 0.05$) between groups.

3. RESULTS

3.1. GelMA synthesis and characterization

To obtain photopolymerizable GelMA polymers with different DM, we varied the concentrations of MA added during synthesis. Examples for ^{1}H NMR spectra of non-methacrylated and methacrylated gelatin are shown in Fig 1a and b, respectively. Comparing the spectra of gelatin and GelMA new signals can be observed at 5.3 ppm and 5.5 ppm, corresponding to the two protons of methacrylate double bond. Therefore we confirmed that MA has been successfully grafted to the gelatin molecules. Quantitative ^{1}H NMR analysis were used to determine the DM (*i.e.*, actual percentages of methacrylation groups functionalized to original free amino groups in gelatin).[24] By varying the mass/volume ratios of MA/gelatin (w/v), variable DM were obtained. Table 1 shows that mass/volume ratios of 0.08, 0.40 and 1.00 yielded three batches of GelMA with low (51.1%), medium (69.5%) and high (89.4%) degrees of methacrylation, respectively, demonstrating the ability to create customized GelMA polymers. The surface charge of the anionic gelatin introduced with various amounts of MA was analyzed in terms of zeta potential. As expected, the net surface charge of GelMA was all

reasonably negative at pH 7.4 due to the presence of high percentage of carboxylate groups in the acidic protein. Despite positive amine groups in the gelatin are consumed by MA upon this derivatization, increasing its methacrylation level increased the z-potential values: -15.84±1.33 mV (Low-GelMA), -11.67±1.39 mV (Medium-GelMA) and -3.81±1.32 mV (High-GelMA). This unexpected result may be explained by the fact that the carboxylate group (−COOH) of gelatin hydrogen bonds (O−H···:O) to carbonyl group (−C=O) of MA, making its deprotonation more difficult at basic pH.[27] Only if a carboxyl group is deprotonated, its conjugate base forms a negatively charged carboxylate anion.

3.2. Mineralization of GelMA hydrogel scaffolds

The photocrosslinked hydrogel scaffold was transparent before mineralization, and became white and opaque due to uptake of mineral after mineralization (Fig. 2a). At the microscopic level, the non-mineralized hydrogels always showed macroporous structure with smooth surfaces while lyophilized (Fig 2b). After mineralization for 12 days, the surface of hydrogel was fully and uniformly covered with spherical agglomerates of minerals, and retained the 3D microstructure of the GelMA framework (Fig 2c). It was noted that the magnified image revealed the presence of hemispherical nodules embedded within mineralized hydrogel matrix, which implied that the minerals nucleation started with the generation of aggregates of CaP prenucleation clusters within the hydrogel matrix as a result of its swelling behavior in mineralized solution (Fig 2d). The observed morphology also indicated that there was strong interactions between hydrogel substrate and biominerals, thus strong adherence of the hydroxyapatite particles to the hydrogel could be achieved. High-magnification (up to 20000x) SEM images revealed that the

spherical agglomerates have a lath-like structure, typically found in natural hydroxyapatite crystals (Fig 2e).[1] EDX spectroscopy confirmed the presence of calcium (Ca) and phosphorus (P) elements in the spherical agglomerates (Fig 2f). As expected, no calcium or phosphate was observed in the non-mineralized hydrogels (see Fig S1 in ESI).

To characterize the structure of the deposited CaP agglomerates within the GelMA hydrogels, multiple analytical tools were performed on crushing mineralized samples in liquid nitrogen. TEM analysis revealed that the inorganic agglomerates consisted of plate-like nanocrystals (Fig 3a). SAED analysis confirmed that the plate-shaped nanocrystals were hydroxyapatite (Fig 3b). The diffraction pattern of the CaP agglomerates grown within GelMA hydrogel exhibited arc shaped patterns along the (002) diffraction plane, indicating that the amino acid backbone in the gelatin-based organics mediates the directional growth of apatite crystals aligned with their *c* axes parallel to the surface of GelMA hydrogel, a phenomenon that is the same as that found in the natural growth of biominerals.[1] A thick and apparently continuous diffraction band containing the 211, 112, and 300 triple diffraction peaks, which are characteristic to biological apatite. The results obtained from the XRD datas were consistent with the morphological observations and the electron diffraction analyses obtained by TEM (Fig 3c). Compared with the reference XRD data of hydroxyapatite (PDF#54-0022) from the International Centre for Diffraction Data (ICDD) database, X-ray diffraction analysis proved that the CaP phase deposited on GelMA was hydroxyapatite rather than octacalcium phosphate, the crystal structure of which is very similar to hydroxyapatite. Note that the apatite phase was poorly crystallized, as shown by weak splitting of the

peaks (particularly between (211) and (112)). This was attributed to the low crystallinity, which is usually observed in the organic-mediated crystallization of an apatite.[28]

The formation of hydroxyapatite onto GelMA hydrogel was further analyzed by FTIR (Fig 3d). Before the growth of hydroxyapatite, the pure hydrogel exhibited the typical amide bands of gelatin protein, including N–H stretching at 3310 cm^{-1} for the amide A, C–H stretching at 3063 cm^{-1} for amide B, C=O stretching at 1657 cm^{-1} for amide I, N–H deformation at 1555 cm^{-1} for amide II and N–H deformation at 1239 cm^{-1} for amide III band, were visible.[29] After mineralization, several new chemical bands associated the crystalline hydroxyapatite appeared, particularly PO_4: the bending modes at 601 and 575 cm^{-1} ($\nu 4$) and the anti-symmetric stretching vibration at 1019 cm^{-1} ($\nu 3$). In addition, a shoulder appeared at 878 cm^{-1} that is attributed to the out-of plane bending adsorption for CO_3^{2-} ($\nu 2$), which indicated that the partial substitution of PO_4^{3-} with CO_3^{2-} groups, within the CaP crystal lattice, thus suggesting the formation of B-type carbonated hydroxyapatite (CHA). The phase and structural data of the mineralized hydrogel were similar to those of the mineralized collagen biomimetic material, as well as to those of natural bone matrix.[30, 31]

Cross-sectional morphological analysis on the mineralized GelMA hydrogels with demonstrated that much smaller spherical hydroxyapatite clusters were observed on the interior of the specimen as opposed to the surface (Fig 4a, b and d). It seems that a mineral penetration of about 180 μm depth occurred on only one side of the scaffold with highly microporous structure. This could be the result of the specimen resting on the bottom of the reaction vessel and one side being more exposed to the mineralization solution than the other. EDS line-scans showed that Ca and P were uniformly distributed

along the mineralized regions (near the top surfaces) (Fig 4c). Aiming to increase the mineral penetration, hydrogel samples were treated with mSBF for up to 3 weeks. However, prolonging the soaking time of treated with mineralization solution was not helpful for further improvement in mineral penetration (data not shown). This may have been caused by regions of solidified mineral potentially blocking further infiltration of the CaP precursor, thus limiting the ultimate depth of penetration. Nevertheless, smaller specimen dimensions (*ie*, thickness) were expected to have the probability of mineral reaching across the entire sample cross-section.

3.3. Effect of the degree of methacrylation on Mineralization of GelMA hydrogels

The swelling characteristics of a network are important for mineralization as it affects solute diffusion and surface properties. The DM is correlated to the cross-link density and a higher DM results in the formation of hydrogels with denser network. Therefore, an increasing amount of methacrylate groups in the feed composition is expected to enhance the density of the network and subsequently reduce the degree of swelling. In the present study, the swelling tests were performed on the GelMA gels samples in PBS are shown in Fig. 5. The mass swelling ratio increased significantly with decreasing DM, further demonstrating that the DM can significantly influence the gel's ability, and propensity, for adsorbing water within the polymer network.

GelMA hydrogel scaffolds with various DM were mineralized with the mSBF for 6 days. Fig 6a, d and g show optical images of mineralized hydrogels with low, medium and high DM, in the wet state, respectively. The three mineralized hydrogels take on a distinctly different appearance with physical changes evident even at the macroscopic level, including the color and rigidity. The Low-GelMA hydrogel exhibited a pure white

color, implying the 3D homogeneous infiltrated mineralization (Fig 6a). Medium-GelMA hydrogel samples showed a marked decrease in their white pigmentation and opacity, as well as a decreased stiffness (Fig 6g). The results were in accordance with the observations from TGA analysis, which confirmed specimen (Medium-GelMA) contains 24.7 wt. % less mineral than specimen (Low-GelMA). In contrast, the High-GelMA hydrogel showed heterogeneous mineral infiltration, with highly mineralized areas appearing white, and less mineralized areas appearing less white and more translucent.

The distribution and the extent of mineralization of the hydrogel matrix with different DM were further analyzed using microscopic examination with SEM-EDS. All hydrogels exhibited mineral deposition to some degree. At higher magnification, morphological differences in the deposited mineral phases on these three hydrogel surfaces become evident (Fig 6). A large number of spherical CaP clusters were compactly deposited on the surface of Low-GelMA hydrogels (Fig. 6b and c), appearing continuous layers. For Medium-GelMA hydrogels, some spherical agglomerates with similar diameter appeared to be accumulated onto the gel, and the mineral layer was not continuous (Fig 6e and f). However, Fig 6h and i show many fewer agglomerates found randomly distributed along the surface of High-GeMA hydrogel (Fig 6h and i). This observation could partially account for the difference in actual amount of mineral deposited in these three hydrogel scaffolds. In particularly, both Medium-GelMA (Fig 6f) and High-GelMA (Fig 6i) showed the formation of mineral nodules, which were actually regions of partial mineral penetration (confirmed by EDS spot analysis indicating the presence of calcium and phosphate). We believed the nodules formed because the infiltration of the precursor ion into the hydrogel matrix is not uniform, and the precursor may infiltrate some portions of

the matrix before others. This phenomenon is most evident in the initial stages of mineralization. As the hydrogels become completely mineralized, nodules are no longer observed since the hydrogels become completely covered with mineral phase, as shown in Fig 6a-c. The average Ca/P ratio of the CaP agglomerates as determined by EDS analysis, was found to be 1.32, 1.50, and 1.62 for mineralized hydrogels with low, medium and high DM, respectively, which are all below the theoretical ratio of hydroxyapatite (Ca/P=1.67), indicating that the apatites is calcium deficient, possibly involving cation substitutions at the Ca^{2+} sites, and/or the substitution at PO_4^{3-} sites by HPO_4^{2-} ions.[32, 33]

XRD analyses revealed that, while analysis of phases formed on all three hydrogels yielded multiple peaks corresponding to hydroxyapatite, mineralized phases formed on the hydrogels with higher DM appeared less crystalline, as can be seen by the lowering of the intensity of the broad pattern (Fig 7a). The amorphous feature was further supported by FTIR data (Fig 7b). The broad, relatively unresolved phosphate bands at 590-610 cm^{-1} and around 1000 cm^{-1} are indicative of poor crystallinity of the mineral in the High-GelMA sample, whereas the characteristic splitting of corresponding phosphate bands into peaks at 565/605 and 1050/1100 cm^{-1} for the Low-GelMA or Medium-GelMA samples further suggested that the extent of mineralization of gels decreased with increasing DM.[34-36]

Thermal analysis of the mineralized hydrogels was done by TGA/DSC. As shown in Fig 8, the three major episodes of derivative weight loss were observed in all the TGA runs, including elimination of physisorbed water at low temperature from 20-200 ℃, the decomposition of organic components from 200-450 ℃ and combustion of the residual

organic matrix from 450-600 ℃. Accordingly, the inorganic phase primarily accounts for the remaining weight of mineralized hydrogels when heated to 600 ℃. Despite the inorganic phase might also have a slight weight loss during the final heating process, which is attributed to the release of CO_2 from carbonated apatite.[37] There was a significant decrease in the extent of mineralization in the hydrogels with an increase in DM. At mineralized for days 6 in mSBF, TGA quantitative analysis of the Low-GelMA hydrogels resulted in a mineral contents of 39.5 wt %, which decreased to 24.7 % and 18.8 wt % for Medium-GelMA and High-GelMA hydrogels, respectively. Only in the case of the former hydrogels, there was a significant increase in the mineral content as a function of time in mSBF. In addition, the direct quantifications of the level of mineral content using an electronic balance further corroborated the TGA data (see Fig S2 in ESI). This high-temperature exothermic peak was found to shift to lower temperatures as the DM of gels decreased, as shown by the exothermic DSC signal (see Fig S3 in ESI), indicating mineralized gel with lower DM has a lower combustion temperature (the last high temperature transition). The results demonstrated more hydroxyapatite crystals embedded within the hydrogel with lower DM are intimately associated and alter the gel's thermal stability.[38]

3.4. Effect of mineralization on scaffold compressive mechanical properties

Because of the coexistence of different infiltrated minerals, changes in the mechanical properties of the composites are to be expected. Thus, unconfined compression test was performed to investigate the effect of mineralization on the mechanical properties of GelMA hydrogels with low, medium, and high DM using samples in the wet (swollen in PBS) state. Fig 9a, b and c show representative stress-strain (S-S) curves of the Low-

GelMA, medium-GelMA and High-GelMA hydrogels, as made, and at days 6 and 12 in mSBF, respectively. All samples presented a similar S-S pattern, with an initial linear elastic region, followed by a region of exponential increase in stress with strain. Compare to pure hydrogel (as made), the mineralized hydrogel composite exhibited a higher initial slope (*i.e.* compressive modulus), maximum compressive stress (*i.e.* compressive strength) and area under the curve (*i.e.* toughness) at 50% deformation. This was attributed to the infiltrated hydroxyapatite minerals integrating well with the GelMA hydrogels by adopting the efficient inorganic-organic composite.

Fig 9d summarizes the evolution of compressive modulus of hydrogels with low, medium and high DM as a function of time in mSBF. The compressive modulus of the all mineralized hydrogels were similar to those found in native tissue environments such as muscle (8-17 kPa) and osteoid matrix (25-40 kPa) . There was a significant increase in the compressive modulus of Low-GelMA and Medium-GelMA hydrogels with conditioning time in mSBF, demonstrating an increase from 5.51±0.8 kPa and 10.62±1.06 kPa, as made, to 15.09±0.61 kPa and 18.84 ±2.91 kPa at days 6 in mSBF, respectively. In contrast, the compressive modulus of High-GelMA hydrogels showed no statistically significant differences ($p > 0.05$) until days 14 in mSBF. It was concluded that the extent of change in the compressive mechanical properties as a function of conditioning time in mSBF was also influenced by DM, which also indicated higher mineral content resulted in enhanced mechanical properties.

4. DISCUSION

Hydrogels are interesting for mimicking biological scaffolds. They can be adjusted to meet specific mechanical and functional requirements of the body by appropriate choice

of monomers and crosslinkers, and the combination of materials. As such, hydrogels are ideal models for studying the basics of biomineralization or for the synthesis of new, advanced organic/inorganic hybrids for bone tissue engineering applications. Indeed, the use of polymeric hydrogels is now common practice for calcium phosphate deposition. For instance, the incorporation of the bioactive glass enhanced the reactivity towards mineral and resulted in a mineralized gel suitable for ready-to-be implanted constructs for cell delivery.[39] The peptide-based hydrogel with mineral-directing sequence were also designed that directed the formation of hydroxyapatite.[40] But all of these studies fundamentally use the same approach: introducing nucleation sites into synthetic hydrogels to induce CaP nucleation. In the present study, we have demonstrated that the suitability of a photocrosslinkable gelatin methacrylate (GelMA) hydrogel for template-driven mineralization utilized anionic residue of gelatin. Heterogeneous nucleation and growth of carbonated apatite with low crystallinity occurred on the surfaces and within the interior of GelMA hydrogels, based on the specific anionic gelatin selected.

Crosslinking of gelatin using crosslinker has been utilized to create gelatin hydrogels that are stable at physiological conditions, more resistant to hydrolytic and enzymatic degradation, and mechanically robust. This study also demonstrated that the chemical crosslinker content of the hydrogel as a parameter regulated the growth of minerals. This is due to the fact that the changes in physicochemical characteristics may influence kinetics of the mineralization process. We observed that the hydrogels with the lowest DM (Low-GelMA) exhibited the highest mineral content under identical conditions (more than two times higher than High-GelMA in mineral content). Modifying on gelatin molecules to introduce crosslinker is a process involving the water-soluble MA to react

with free amine groups of lysine or hydroxylysine residues, while hydrogen bond to carboxylic groups of aspartic or glutamic acid. As the crosslinker content, DM, increases, more free amino and carboxylate groups are consumed, a significant reduction in surface charges of the gel was shown by the zeta-potential measurements. Therefore, the nucleation of minerals was suppressed by increasing the crosslinker content, which can be partially explained by charge−charge interactions. Binding sites for calcium ions adsorption were predominantly carboxylates, while phosphate ions bound to the amino group of lysine side chains.[42, 43] An increase in the DM implies a decrease in the charge concentration (number of charge per mass) of the hydrogel, which cannot afford to attract more Ca^{2+} or PO_4^{3-} ions. This would increase the interfacial energy between the gel and calcium phosphate and in turn inhibit the initial nucleation of mineral phases, in accordance with the Gibbs law. This observation is consistent with previous biomineralization study demonstrated that mineralization could be controlled by modifying the density of negatively charged groups in the hydrogel.[22] It was suggested that interactions between positive calcium ions and negatively charged carboxylic groups in the gels are the driving force for mineralization.

In addition, the chemical crosslinker content can significantly influence the mineralization outcome, which was also interpreted that the DM had a significant effect on the solute diffusibility of the hydrogels. With a higher DM, the hydrogel network is denser. The swelling measurements showed that the water adsorption capacity of the gels was reduced with increasing DM. The limited water diffusion for hydrogel hinders the infiltration of the precursor ions, thereby increasing the interfacial energy. Conversely, the loosely crosslinked hydrogels have likely allowed better diffusion of precursor ions or

pre-nucleation ion clusters, thereby replenishing precursor ions. The mineral nucleation and growth in a timely manner to sustain a higher supersaturation of calcium and phosphate within the gel microenvironment can result in a fast mineral growth rate.[44] In addition, the significant increase in volume of the swollen hydrogel may have further facilitated anionic gelatin-mediated active infiltration of precursor ions and more sustained growth of mineral domains. Furthermore, in supersaturated mineralization solution, a surface with higher wettability enables better coverage of gel and significantly accelerates nucleation and precipitation which in turn accelerate the apatite nucleation and precipitation process.[45] These interpretations suggested that swelling properties of the gel matrix imparts the CaP deposition both kinetically and thermodynamically.

Mineralization through mSBF conditioning and DM of GelMA hydrogels coordinated affected the mechanical properties of the scaffolds, and resulted in a transition from a soft to hard tissue-like response to compressive stress. The slope of line-region of the S-S curves of High-GelMA increased when compared to that of the Low-GelMA, because cross-linking chemical reaction improves the mechanical stability of the hydrogels. A further increase in the compressive modulus was registered in the all three hydrogels mineralized in mSBF due to the biomimetic incorporation of hydroxyapatite minerals, but differences of gels of lower DM was more significant because of the higher mineral content. While the properties of the composites in the hydrated state could not be used for full load-bearing applications, the mineralized hydrogels have enough mechanical integrity and cytocompatibility as a vehicle for sustained release of growth factors and to be used as bone-void fillers.

Many previous studies have also described that hydrogel can obtain high stiffnesses by increasing chemical crosslinking agents content.[46-48] However, the high levels of crosslinking agents are often cytotoxic or elicit immunological responses from the host.[19, 49, 50] Moreover, the highly cross-linked nature of the network formed by this way posed limitations in maintaining cell viability. Currently, although enhancing the stiffness and while maintaining the cytocompatibility for hydrogels still remain as a challenge, our observation about the higher calcification ability corresponding to low crosslinker content is believed to overcome the limitations. Furthermore, the effects of crosslinker on the mineralization outcome of hydrogels may also be translated to mineral-polymer composite materials made by other macromolecules and synthetic polymers associated with biomineralization, thus impacting the hydrogel mineralization engineering processes.

5. CONCLUSIONS

In the present study, we have demonstrated that GelMA hydrogel can serve as an organic template for 3D hydroxyapatite-mineralization. The hydroxyapatite nanocrystals were found to be distributed in the scaffold, where both surface and internal mineralization was accomplished. The charged functional groups in gelatin structure have likely played a critical role in facilitating active infiltration of oppositely charged precursor ions or pre-nucleation ion clusters and lowering the interfacial energy for heterogeneous nucleation and growth. Furthermore, the mineralization outcome of the GelMA hydrogel, including the extent, composition, and distribution of the templated minerals grown within the hydrogels, can be readily controlled depending on

methacrylation levels. In particular, a higher levels of methacrylation corresponded to a decrease in gel mineralization extent, and lower crystalline carbonated hydroxyapatite was found formed within hydrogels with in higher levels of methacrylation. We believed that crosslinker in the GelMA hydrogel suppressed mineralization through consuming free charges, and inhibiting the infiltration of precursor ions, thus reducing the enthalpic interaction between the matrix and minerals, leading to decreased mineral deposition. In addition, biomimetically mineralized GelMA hydrogel scaffolds with high mineral content exhibited better load-bearing properties when compared to the use of non-mineralized polymeric scaffolds.

ASSOCIATED CONTENT

Corresponding Author

*E-mail: tanguoxin@126.com (G.T.); imcyning@scut.edu.cn (C.N.)

Notes

The authors declare no competing financial interest.

ACKNOWLEDGMENT

(The authors gratefully acknowledge the financial support of National Basic Research Program of China (Grant Nos. 2012CB619100), the National Natural Science Foundation of China (Grant No. 51372087, 51072055).

REFERENCES

1. M. J. Olszta, X. Cheng, S. S. Jee, R. Kumar, Y.-Y. Kim, M. J. Kaufman, E. P. Douglas and L. B. Gower, *Mater. Sci. Eng., R*, 2007, 58, 77-116.

2. N. M. Alves, I. B. Leonor, H. S. Azevedo, R. L. Reis and J. F. Mano, *J. Mater. Chem.*, 2010, 20, 2911.
3. T. E. Douglas, P. B. Messersmith, S. Chasan, A. G. Mikos, E. L. de Mulder, G. Dickson, D. Schaubroeck, L. Balcaen, F. Vanhaecke, P. Dubruel, J. A. Jansen and S. C. Leeuwenburgh, *Macromol Biosci.*, 2012, 12, 1077-1089.
4. L. Klouda, K. R. Perkins, B. M. Watson, M. C. Hacker, S. J. Bryant, R. M. Raphael, F. K. Kasper and A. G. Mikos, *Acta Biomater.*, 2011, 7, 1460-1467.
5. C. Yan, M. E. Mackay, K. Czymmek, R. P. Nagarkar, J. P. Schneider and D. J. Pochan, *Langmuir*, 2012, 28, 6076-6087.
6. K. Chatterjee, S. Lin-Gibson, W. E. Wallace, S. H. Parekh, Y. J. Lee, M. T. Cicerone, M. F. Young and C. G. Simon, Jr., *Biomaterials*, 2010, 31, 5051-5062.
7. S. S. Lee, B. J. Huang, S. R. Kaltz, S. Sur, C. J. Newcomb, S. R. Stock, R. N. Shah and S. I. Stupp, *Biomaterials*, 2013, 34, 452-459.
8. D. Seliktar, *Science*, 2012, 336, 1124-1128.
9. K. Y. Lee and D. J. Mooney, *Chem Rev.*, 2001, 101, 1869-1880.
10. A. Khademhosseini and R. Langer, *Biomaterials*, 2007, 28, 5087-5092.
11. C. Fan, C. Zhang, Y. Jing, L. Liao and L. Liu, *RSC Adv.*, 2013, 3, 157.
12. M. O. Wang, J. M. Etheridge, J. A. Thompson, C. E. Vorwald, D. Dean and J. P. Fisher, *Biomacromolecules*, 2013, 14, 1321-1329.
13. D.-M. Dragusin, S. Van Vlierberghe, P. Dubruel, M. Dierick, L. Van Hoorebeke, H. A. Declercq, M. M. Cornelissen and I.-C. Stancu, *Soft Matter.*, 2012, 8, 9589.
14. J. F. Mano, R. A. Sousa, L. F. Boesel, N. M. Neves and R. L. Reis, *Compos. Sci. Technol.*, 2004, 64, 789-817.
15. M. Persson, G. S. Lorite, S.-W. Cho, J. Tuukkanen and M. Skrifvars, *ACS Appl Mater Interfaces*, 2013, 5, 6864-6872.
16. H. W. Kim, J. H. Song and H. E. Kim, *Adv. Funct. Mater.*, 2005, 15, 1988-1994.
17. K. Bleek and A. Taubert, *Acta Biomater.*, 2013, 9, 6283-6321.
18. W. Zheng, W. Zhang and X. Jiang, *Adv. Eng. Mater.*, 2010, 12, B451-B466.
19. J. W. Nichol, S. T. Koshy, H. Bae, C. M. Hwang, S. Yamanlar and A. Khademhosseini, *Biomaterials*, 2010, 31, 5536-5544.
20. P. Zhu, Y. Masuda and K. Koumoto, *Biomaterials*, 2004, 25, 3915-3921.
21. E. Beniash, A. S. Deshpande, P. A. Fang, N. S. Lieb, X. Zhang and C. S. Sfeir, *J Struct Biol.*, 2011, 174, 100-106.

22. C. Cha, E. S. Kim, I. W. Kim and H. Kong, *Biomaterials*, 2011, 32, 2695-2703.
23. A. I. Van Den Bulcke, B. Bogdanov, N. De Rooze, E. H. Schacht, M. Cornelissen and H. Berghmans, *Biomacromolecules*, 2000, 1, 31-38.
24. A. Ovsianikov, A. Deiwick, S. Van Vlierberghe, P. Dubruel, L. Moller, G. Drager and B. Chichkov, *Biomacromolecules*, 2011, 12, 851-858.
25. T. Kokubo and H. Takadama, *Biomaterials*, 2006, 27, 2907-2915.
26. S. Weiner and W. Traub, In *Mechanisms and Phylogeny of Mineralization in Biological Systems*, ed. S. Suga, H. Nakahara, Springer-Verlag, New York, 2nd edn., 1991, vol. 10, pp. 247.
27. J. Y. Lee, P. C. Painter and M. M. Coleman, *Macromolecules*, 1988, 21, 954-960.
28. S. Weiner and L. Addadi, *J. Mater. Chem.*, 1997, 7, 689-702.
29. M. C. Chang and J. Tanaka, *Biomaterials*, 2002, 23, 4811-4818.
30. B. Marelli, C. E. Ghezzi, J. E. Barralet and S. N. Nazhat, *Soft Matter.*, 2011, 7, 9898.
31. M. Kikuchi, T. Ikoma, S. Itoh, H. N. Matsumoto, Y. Koyama, K. Takakuda, K. Shinomiya and J. Tanaka, *Compos. Sci. Technol.*, 2004, 64, 819-825.
32. G. Tan, L. Zhou, C. Ning, Y. Tan, G. Ni, J. Liao, P. Yu and X. Chen, *Appl Surf Sci.*, 2013, 279, 293-299.
33. Y. F. Chou, W. A. Chiou, Y. Xu, J. C. Dunn and B. M. Wu, *Biomaterials*, 2004, 25, 5323-5331.
34. C. Combes and C. Rey, *Acta Biomater.*, 2010, 6, 3362-3378.
35. R. J. Dekker, J. D. de Bruijn, M. Stigter, F. Barrere, P. Layrolle and C. A. van Blitterswijk, *Biomaterials*, 2005, 26, 5231-5239.
36. D. Tadic, F. Peters and M. Epple, *Biomaterials*, 2002, 23, 2553-2559.
37. L. N. Niu, K. Jiao, H. Ryou, C. K. Yiu, J. H. Chen, L. Breschi, D. D. Arola, D. H. Pashley and F. R. Tay, *Angew Chem Int Ed Engl.*, 2013, 52, 5762-5766.
38. L. Lozano, M. Pena-Rico, A. Heredia, J. Ocotlan-Flores, A. Gomez-Cortes, R. Velazquez, I. Belio and L. Bucio, *J. Mater. Sci.*, 2003, 38, 4777-4782.
39. B. Marelli, C. E. Ghezzi, D. Mohn, W. J. Stark, J. E. Barralet, A. R. Boccaccini and S. N. Nazhat, *Biomaterials*, 2011, 32, 8915-8926.
40. M. Gungormus, M. Branco, H. Fong, J. P. Schneider, C. Tamerler and M. Sarikaya, *Biomaterials*, 2010, 31, 7266-7274.
41. J. Li, Y. Chen, Y. Yin, F. Yao and K. Yao, *Biomaterials*, 2007, 28, 781-790.

42. R. J. Coleman, K. S. Jack, S. b. Perrier and L. Grøndahl, *Cryst Growth Des.*, 2013, 13, 4252-4259.
43. W. J. Landis and R. Jacquet, *Calcif Tissue Int.*, 2013, 93, 329-337.
44. S. Mann, In *Biomineralization: principles and concepts in bioinorganic materials chemistry*, Oxford University Press, New York, 4nd edn., **2001**, pp. 43.
45. A. Walton, In: *Nucleation,* ed. A, Zettlemoyer, Decker, New York, **1969**, pp. 225.
46. D. F. Coutinho, S. V. Sant, H. Shin, J. T. Oliveira, M. E. Gomes, N. M. Neves, A. Khademhosseini and R. L. Reis, *Biomaterials*, 2010, 31, 7494-7502.
47. H. Bae, A. F. Ahari, H. Shin, J. W. Nichol, C. B. Hutson, M. Masaeli, S. H. Kim, H. Aubin, S. Yamanlar and A. Khademhosseini, *Soft Matter.*, 2011, 7, 1903-1911.
48. S. A. Bencherif, A. Srinivasan, F. Horkay, J. O. Hollinger, K. Matyjaszewski and N. R. Washburn, *Biomaterials*, 2008, 29, 1739-1749.
49. E. P. Broderick, D. M. O'Halloran, Y. A. Rochev, M. Griffin, R. J. Collighan and A. S. Pandit, *J Biomed Mater Res B Appl Biomater.*, 2005, 72, 37-42.
50. H. C. Liang, W. H. Chang, K. J. Lin and H. W. Sung, *J. Biomed. Mater. Res., Part A*, 2003, 65, 271-282.

Table 1. DM and zeta potential of GelMA as a function of the mass/volume ratios of MA/gelatin

Samples	MA/gelatin (ml/g)	Degrees of methacrylation(DM, %)	Zeta potential[a] (mV)
Low-GelMA	0.08	51.1	-15.84±1.33
Medium-GelMA	0.40	69.5	-11.67±1.39
High-GelMA	1.00	89.4	-3.84±1.32

[a] Values of Zeta potential are mean ± standard deviation (n = 3).

LEGENDS TO FIGURES

Fig 1. NMR characterization of methacrylated gelatin: (a) Representative ^{1}H NMR spectrum of gelatin. (b) Representative ^{1}H NMR spectrum of High-GelMA (DM 89.4%). Vinyl groups of the methacrylic anhydride (MA) were identified at the peaks H_a (5.3 ppm) and H_b (5.5 ppm).

Fig 2. Images of GelMA hydrogel before and after mineralization for 12 days. (a) Photograph of hydrogel scaffold showing color change before and after mineralization. (b) SEM images of unmineralized hydrogel showing porous structures with smooth surfaces. (c-e) SEM images of mineralized hydrogel showing calcium phosphate clusters nucleated on the surface of the gel, (d) and (e) are magnified images from (c), (f) is corresponding Energy Dispersive X-ray (EDX) spectroscopy captured with image (d). Arrows indicate the hemispherical calcium phosphate nodules.

Fig 3. Characteristics of the 12 days mineralized GelMA hydrogel composite: (a) TEM, (b) SAED, and (c) X-ray diffraction show that the calcium phosphate agglomerates are hydroxyapatite crystals. (d) The growth of composite was further investigated by FTIR spectroscopy, the peaks at 1645/1550/1243 cm^{-1} and 575/601/878/1019/3063/3430 cm^{-1} indicate the presence of gelatin and carbonated hydroxyapatite crystals, respectively. Data on the pure unmineralized hydrogel and the documented X-ray diffraction patterns of HA (PDF#54-0022) are presented as reference.

Fig 4. SEM images and EDS line-scans spectra of the cross-section of mineralized GelMA hydrogel. (a) SEM of cross-section of a 12 days mineralized scaffold using GelMA hydrogel with medium DM. (b and d) SEM image of a region of the mineralized scaffold outlined by the rectangle in (a) at increasing magnifications. (c) EDS line scan spectroscopy of the mineral penetrative area of cross-section marked with the red line on the mineralized hydrogel scaffold shown in (a) (yellow brace symbols indicating areas of mineral penetration).

Fig 5. Mass swelling ratio of the methacrylated gelatin hydrogels (n = 4) at various degrees of methacrylation. The hydrogel swelling ratio is calculated by dividing the swollen gel mass by the dry gel mass.

Fig 6. Photograph, SEM images and corresponding EDS spectra (inset) of mineralized GelMA hydrogel samples with varied DM at days 6 in mSBF. (a, d and g) Photograph of mineralized samples with low, medium and high DM, respectively, which show differences in the color, with highly mineralized sample (a) appearing white, and less mineralized sample (g) appearing grey and more translucent. (b, e and f) SEM micrograph at lower magnification of mineralized GelMA hydrogels with low, medium and high DM, respectively, showing the distribution of mineral crystals in the matrix. The morphological differences among the deposited minerals are observable at higher magnifications in panels c, f and i, respectively.

Fig 7. Chemical characterization of mineralized GelMA hydrogel with different mineralization degrees prepared from GelMA scaffolds with varied DM: (a) XRD pattern and (b) FTIR spectrum.

Fig 8. TGA curves of mineralized GelMA hydrogels with varied DM. The GelMA hydrogel samples of low DM (Low-GelMA) at days 7 and day 14 in mSBF were used to investigate the effect of the mineralization time on the mineralization process. The mineral contents (wt.%) of mineralized samples were measured at 600 ℃. The small weight loss beyond this temperature can be attributed to CO_2 loss from carbonated apatite.

Fig 9. The mechanical properties of mineralized hydrogel samples. (a, b and c) Representative compressive stress–strain curves of Low-GelMA, Medium-GelMA and High-GelMA hydrogels, as made, and at days 7 and 14 in mSBF, respectively. (d) Compressive elastic modulus as a function of DM and conditioning time in mSBF was also influenced by DM. (*$p < 0.05$, **$p < 0.01$, ***$p < 0.001$).

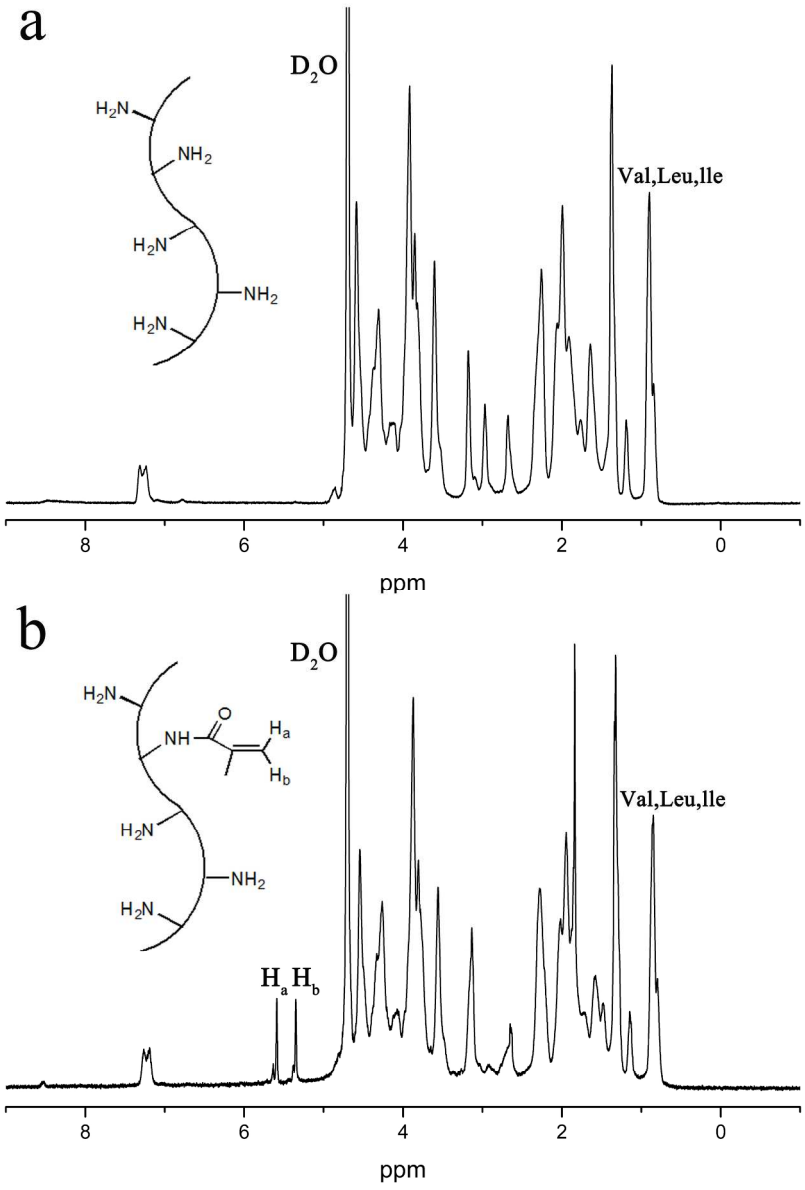

Figure 1

191x280mm (300 x 300 DPI)

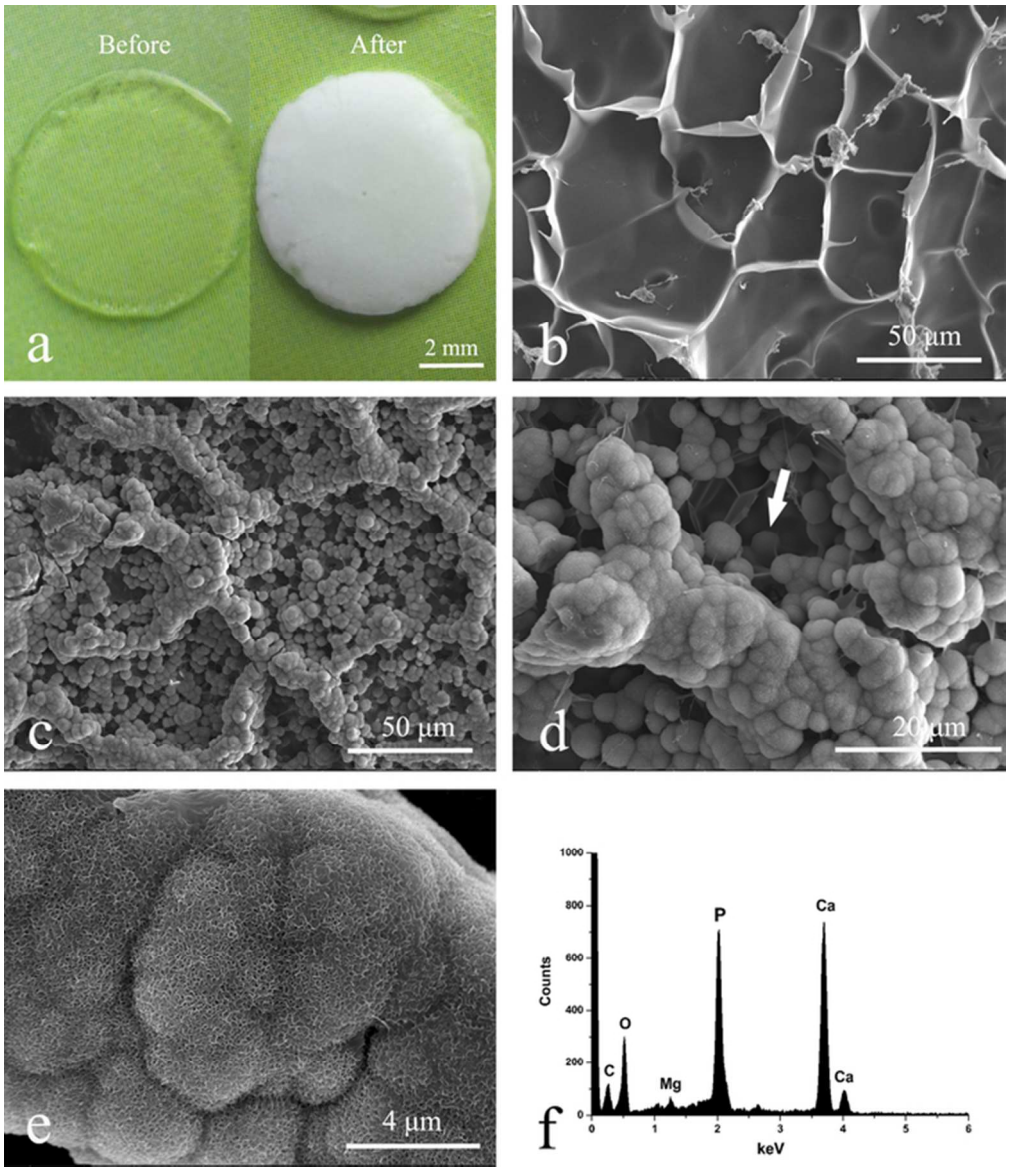

Figure 2
61x71mm (300 x 300 DPI)

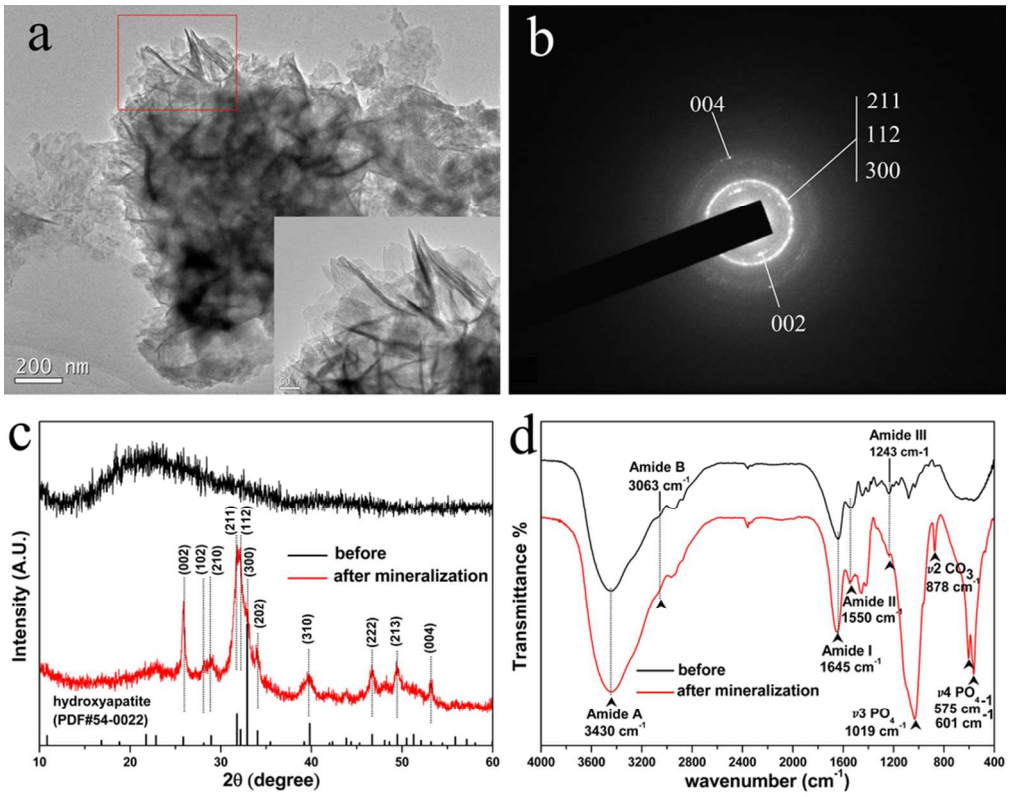

Figure 3
84x68mm (300 x 300 DPI)

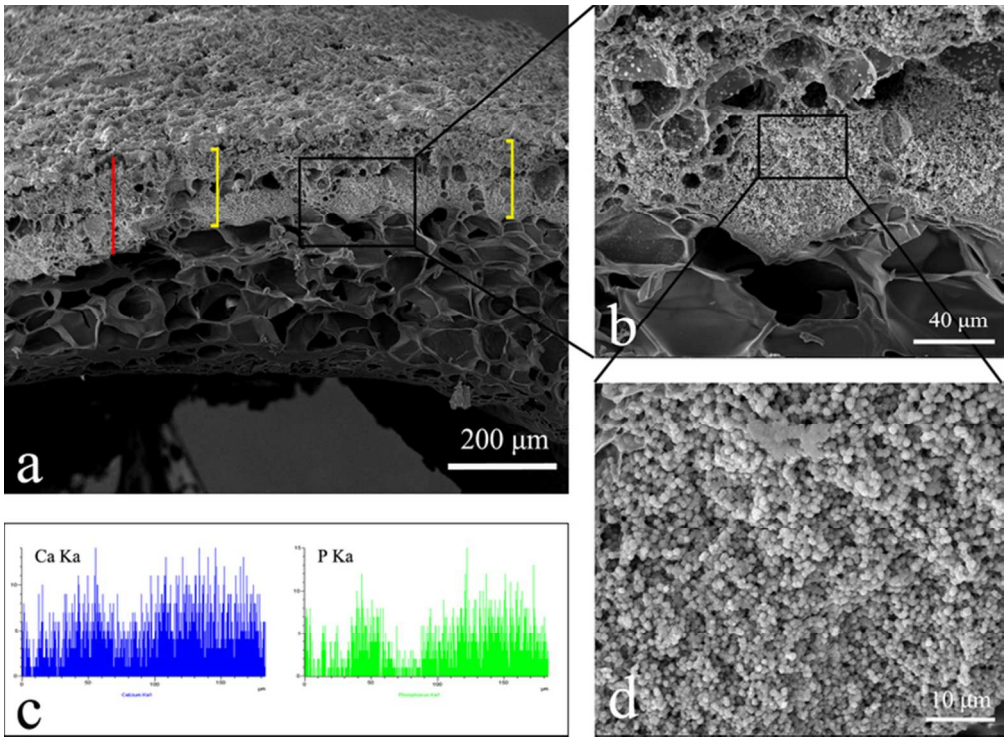

Figure 4
33x24mm (600 x 600 DPI)

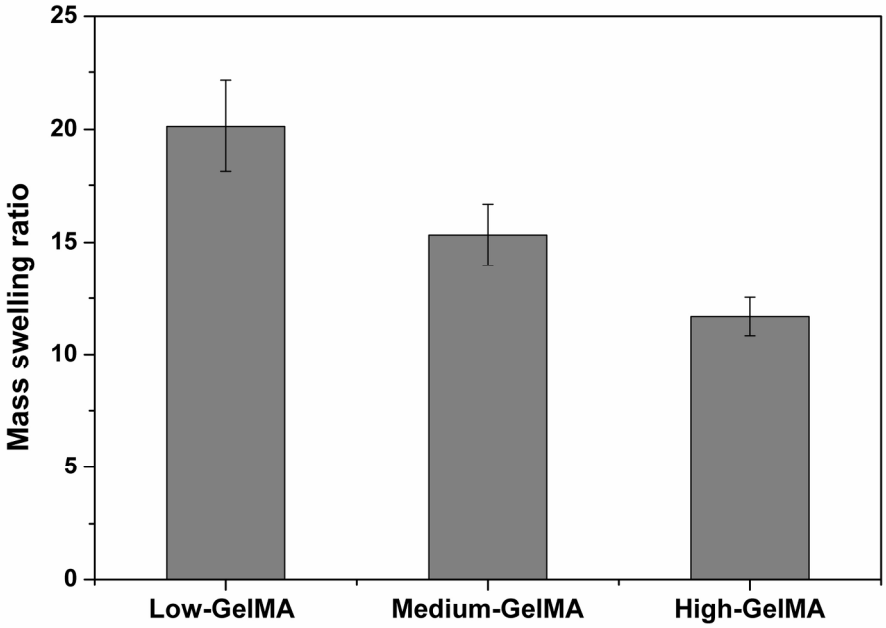

Figure 5
202x142mm (300 x 300 DPI)

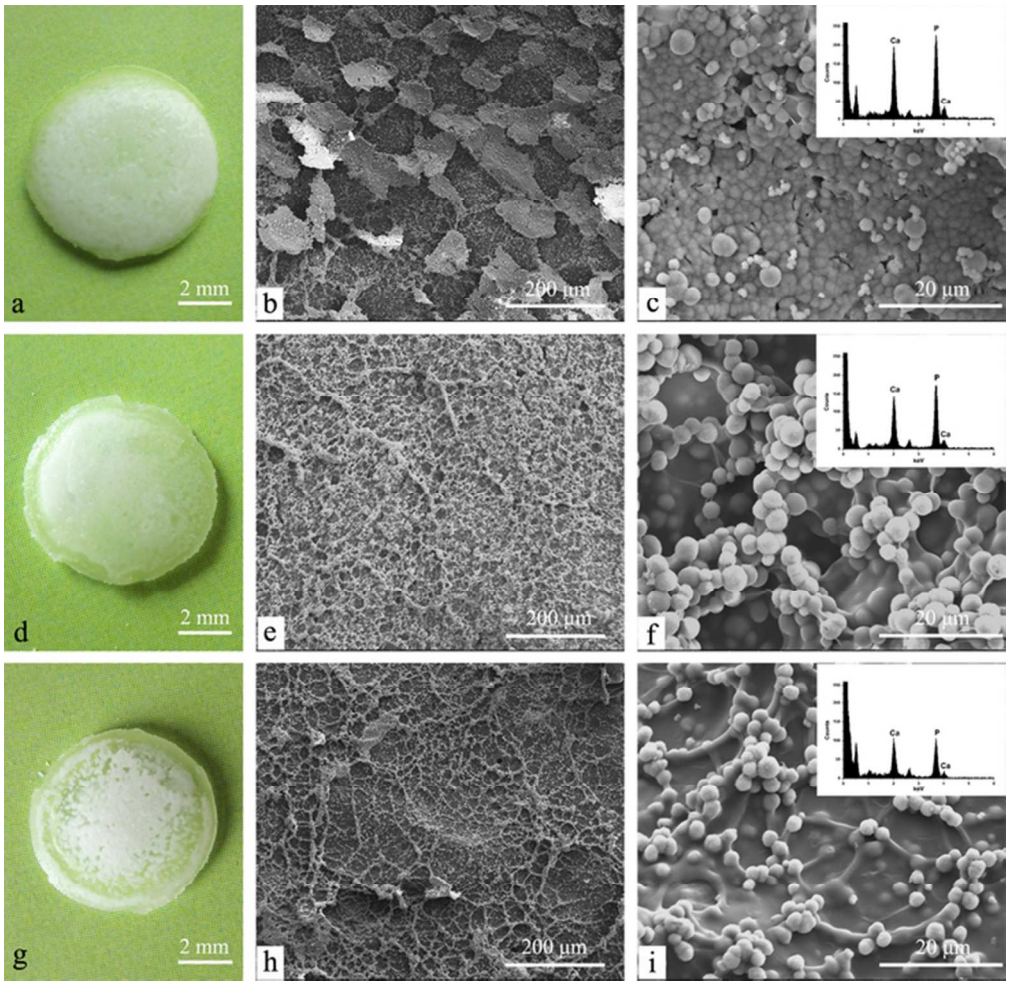

Figure 6
61x60mm (300 x 300 DPI)

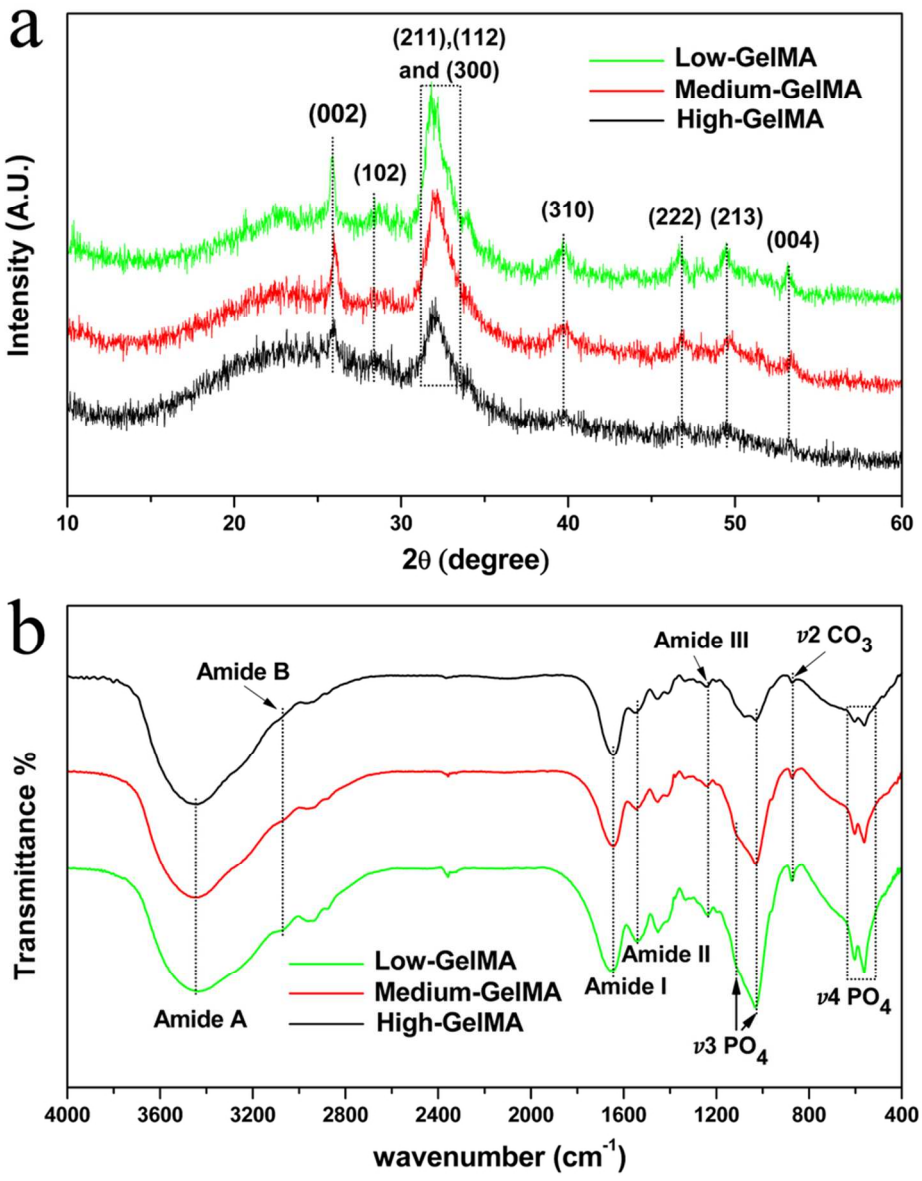

Figure 7
80x102mm (300 x 300 DPI)

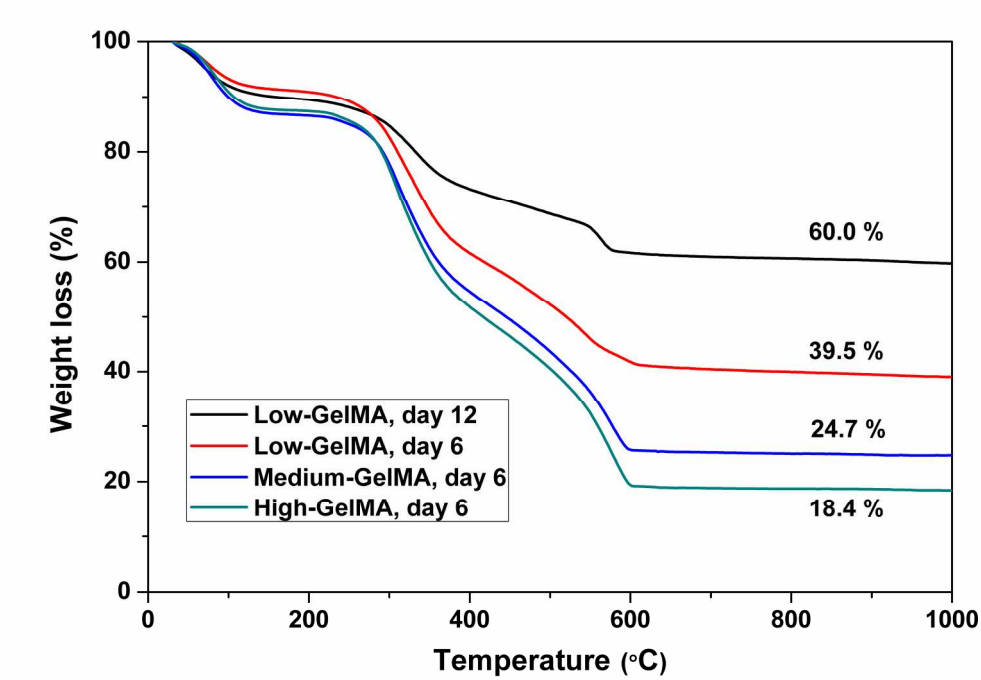

Figure 8
202x142mm (300 x 300 DPI)

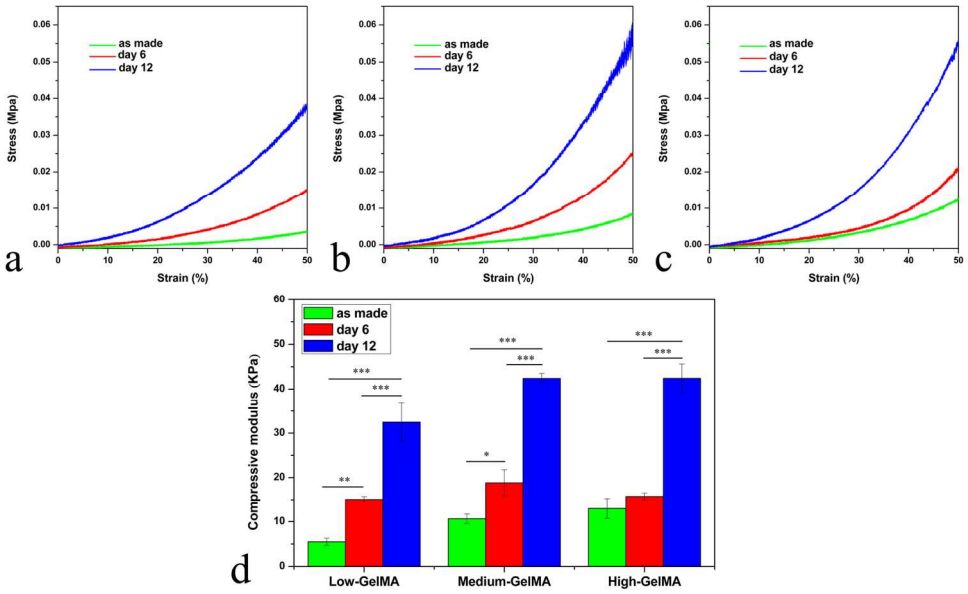

Figure 9
156x96mm (300 x 300 DPI)